FYS5555 Compulsory project 1

Victor Ananyev

February 28, 2020

1 Muon collider

Process In this project we will investigate the process of annihilation of muon and anti-muon pair into b and $\bar{b}$ quarks. At the tree level in the leading order the following three diagrams contribute:

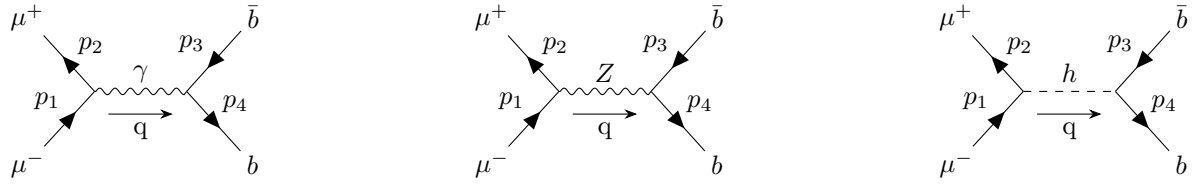

(a) Photon (b) Z (c) Higgs

Figure 1: Feynman diagrams contributing to $\mu^+\mu^- \to b\bar{b}$ at the tree level in the leading order

Out main goal is to explore the behavior of the differential cross-section, total cross-section and forward-backward asymmetry of the process, and learn the role of each diagram contributing to it.

Building matrix element The key quanity common for all observables mentioned above is the matrix element. It assembles all our knowledge about fundamental interactions and is the only quantity which depends on the model parameters. To compute matrix element we draw Feynman diagrams, each representing a term in the Taylor expansion of S-matrix with respect to the coupling constant, and translate each diagram into a mathematical expression. For the process $\mu^-\mu^+ \to b\bar{b}$, based on the diagrams at the tree (lowest) level we get the following matrix element:

$$\mathcal{M} = \mathcal{M}_\gamma + \mathcal{M}_Z + \mathcal{M}_h \tag{1}$$

$$\mathcal{M}_\gamma = \bar{v}(p_2)\mathrm{i}e\gamma^{\mu_1}u(p_1)\ \frac{-\mathrm{i}g_{\mu_1\mu_2}}{q^2}\ \bar{u}(p_3)(-\mathrm{i}Q_b e)\gamma^{\mu_2}v(p_4) \tag{2}$$

$$\mathcal{M}_h = \bar{v}(p_2)\frac{-\mathrm{i}}{2}\frac{g_W}{m_W}m_\mu u(p_1)\ \frac{\mathrm{i}}{q^2-m_h^2}\ \bar{u}(p_3)\frac{-\mathrm{i}}{2}\frac{g_W}{m_W}m_b v(p_4) \tag{3}$$

$$\begin{aligned}\mathcal{M}_Z = {} & \bar{v}(p_2)\frac{-\mathrm{i}g_Z}{2}\gamma^{\mu_1}\left[(-\frac{1}{2}+2\sin^2\theta_w)+\frac{1}{2}\gamma^5\right]u(p_1)\times \\ & \times(-\mathrm{i})\frac{g_{\mu_1\mu_2}-\frac{q^{\mu_1}q^{\mu_2}}{m_Z^2}}{q^2-m_Z^2}\ \bar{u}(p_3)\frac{-\mathrm{i}g_Z}{2}\gamma^{\mu_2}\left[(-\frac{1}{2}-2Q_b\sin^2\theta_w)+\frac{1}{2}\gamma^5\right]v(p_4)\end{aligned} \tag{4}$$

While building the expression for matrix element we used Feynman rules in the notation of Nagashima et al. [15]. Here e is the elementary charge (which numerically is equal to absolute value of the electron charge, but differs in sign), Q_b is the charge of b-quark measured in e units, $(m_W, m_b, m_\mu, m_Z, m_H)$ are masses of the corresponding particles, θ_w is the Weinberg's angle, g_W and g_Z are weak coupling constants. It is important to mention that these parameters are not independent, this is a weakness of the representation from the perspective of the rigorous theory, but at the same time it allows for a flexibility of testing the entire expression separating diagram contributions.

Below we provide the table of numerical values being used in plots and numerics. Values correspond to CompHEP [12] default parameters for SM in Unitary gauge.

Table 1: Model parameters used for calculations (extracted from CompHEP)

m_μ	0.105
m_b	4.85
m_W	80.0
m_h	115.0
m_Z	91.2
e	0.313
Q_b	$-\frac{1}{3}$
$\sin\theta_w$	0.48076
g_W	$\frac{e}{\sin\theta_w} = 0.651$
g_Z	$\frac{e}{\sin\theta_w \cos\theta_w} = 0.742$

To take into account the finite lifetime of massive Z and h in the propagators, we append imaginary term to their propagators, proportional to their decay width:

$$Z: \quad \frac{1}{q^2 - m_Z^2} \to \frac{1}{q^2 - m_Z^2 + \mathrm{i} m_Z \Gamma_Z} \tag{5}$$

$$h: \quad \frac{1}{q^2 - m_h^2} \to \frac{1}{q^2 - m_h^2 + \mathrm{i} m_h \Gamma_h} \tag{6}$$

Corresponding widths were taken from CompHEP:

Table 2: Decay widths used for calculations

Γ_Z	2.43
Γ_h	0.00617

Computation After extending propagators with the decay width terms, we have to square the matrix element (keeping track of interference terms), apply spinor summation identities and gamma matrix traces. To conduct this very technical and involved procedure we developed a special routine based on the FORM [18] package.

FORM allows for easy symbolic calculations with powerful pattern matching capabilities. It simplifies operations with vectors and non-commutative objects (like matrices and operators), keeping track of indices under the hood. The essential part of the package is automated computation of traces of gamma matrices, so that you'll never miss index or term in your QFT computations.

Making use of the FORM's power we developed a simple routine which implements only two operations: complex conjugation of the matrix element and taking the trace with spinor sums. You can find the source code for the abstract package [7] and also its application to the muon annihilation process [6] at our GitHub page. As a cross-check we computed matrix element for $ee^+ \to \mu\mu^+$ and compared to the result given by Peskin and Schroeder [16].

Below we are showing an extract from the differential cross-section. While it is not readable, it makes it obvious why overparametrization of the model comes in handy. Overparametrizaiton helps us to investigate contributions of different terms separately.

```
MsqSimple =
    + t * ( 1/2*mZ^4*gZ^4*s^3*[z, prop]^2 - 2*mZ^4*gZ^4*sW^2*s^3*[z, prop]^2
      + 2*mZ^4*gZ^4*sW^2*Qb*s^3*[z, prop]^2 + 2*mZ^4*gZ^4*sW^4*s^3*
      [z, prop]^2 - 8*mZ^4*gZ^4*sW^4*Qb*s^3*[z, prop]^2 + 2*mZ^4*gZ^4*sW^4*
      Qb^2*s^3*[z, prop]^2 + 8*mZ^4*gZ^4*sW^6*Qb*s^3*[z, prop]^2 - 8*mZ^4*
      gZ^4*sW^6*Qb^2*s^3*[z, prop]^2 + 16*mZ^4*gZ^4*sW^8*Qb^2*s^3*[z, prop]^2
      - mZ^6*gZ^4*s^2*[z, prop]^2 + 1/2*mZ^6*gZ^4*wZ^2*s*[z, prop]^2 + 4*
      mZ^6*gZ^4*sW^2*s^2*[z, prop]^2 - 4*mZ^6*gZ^4*sW^2*Qb*s^2*[z, prop]^2 -
      2*mZ^6*gZ^4*sW^2*wZ^2*s*[z, prop]^2 + 2*mZ^6*gZ^4*sW^2*wZ^2*Qb*s*
```

```
[z,prop]^2 - 4*mZ^6*gZ^4*sW^4*s^2*[z,prop]^2 + 16*mZ^6*gZ^4*sW^4*Qb*
s^2*[z,prop]^2 - 4*mZ^6*gZ^4*sW^4*Qb^2*s^2*[z,prop]^2 + 2*mZ^6*gZ^4*
sW^4*wZ^2*s*[z,prop]^2 - 8*mZ^6*gZ^4*sW^4*wZ^2*Qb*s*[z,prop]^2 + 2*
mZ^6*gZ^4*sW^4*wZ^2*Qb^2*s*[z,prop]^2 - 16*mZ^6*gZ^4*sW^6*Qb*s^2*
[z,prop]^2 + 16*mZ^6*gZ^4*sW^6*Qb^2*s^2*[z,prop]^2 + 8*mZ^6*gZ^4*sW^6
*wZ^2*Qb*s*[z,prop]^2 - 8*mZ^6*gZ^4*sW^6*wZ^2*Qb^2*s*[z,prop]^2 - 32*
mZ^6*gZ^4*sW^8*Qb^2*s^2*[z,prop]^2 + 16*mZ^6*gZ^4*sW^8*wZ^2*Qb^2*s*
[z,prop]^2 + 1/2*mZ^8*gZ^4*s*[z,prop]^2 - 2*mZ^8*gZ^4*sW^2*s*
[z,prop]^2 + 2*mZ^8*gZ^4*sW^2*Qb*s*[z,prop]^2 + 2*mZ^8*gZ^4*sW^4*s*
[z,prop]^2 - 8*mZ^8*gZ^4*sW^4*Qb*s*[z,prop]^2 + 2*mZ^8*gZ^4*sW^4*Qb^2
```

Listing 1: Differential cross-section. FORM output. First 20 lines

Similar expression was produced for the total cross-section. Both of them afterwards were fed to the Jupyter Notebook in order to visualize the dependencies and compare them to CompHEP output. You can find the full notebook at the GitHub [8].

Differential cross-section General expression for the differetial cross section in the center of mass (c.o.m) frame looks as follows [17]:

$$\frac{d\sigma}{dt} = \frac{1}{64\pi s}\frac{1}{|\mathbf{p}_{cm}|}|\mathcal{M}|^2 \tag{7}$$

First of all we plot the differential cross section as a function of $t = (\mathbf{p}_1 - \mathbf{p}_3)^2$, then we apply coordinate change in order to get expression in terms of $\cos\theta = \frac{\mathbf{p}_1 \cdot \mathbf{p}_3}{|\mathbf{p}_1||\mathbf{p}_3|}$.

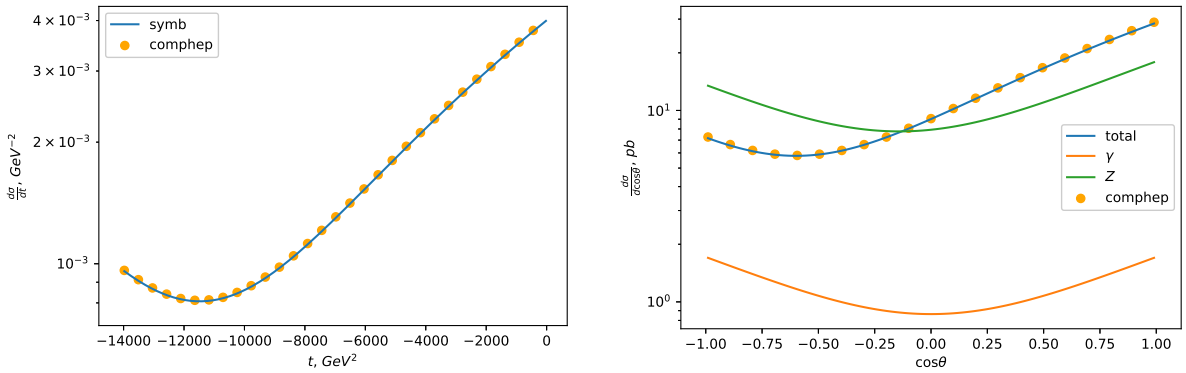

(a) (b)

Figure 2: Differential cross section and contributions of various processes, $s = 120\ GeV$

For the transformation from t to $\cos\theta$ we had to take into account the Jacobian:

$$\frac{dt}{d\cos\theta} = 2\sqrt{\frac{s}{4} - m_\mu^2}\sqrt{\frac{s}{4} - m_b^2} \tag{8}$$

Also $\frac{d\sigma}{d\cos\theta}$ is measured in $pb = 2.56819 \times 10^{-9} GeV^{-2}$. We excluded Higgs process since it is several orders of magnitude smaller then other contributions. The essential effect which can be discovered from the partial contribution plots, is that assymetry is not present in separate channels but being generated only due to the interference.

Total cross section We plot total cross section at different energy scales: *low energy* ($\sqrt{s} < 80\ GeV$), to make electromagnetic contribution and masses of leptons explicit, *high energy* ($\sqrt{s} < 8\ TeV$) to compare large scale behaviors of the processes, finally ranges around Z and H *peaks* to verify that we catch these signs of Standard Model in our calculations.

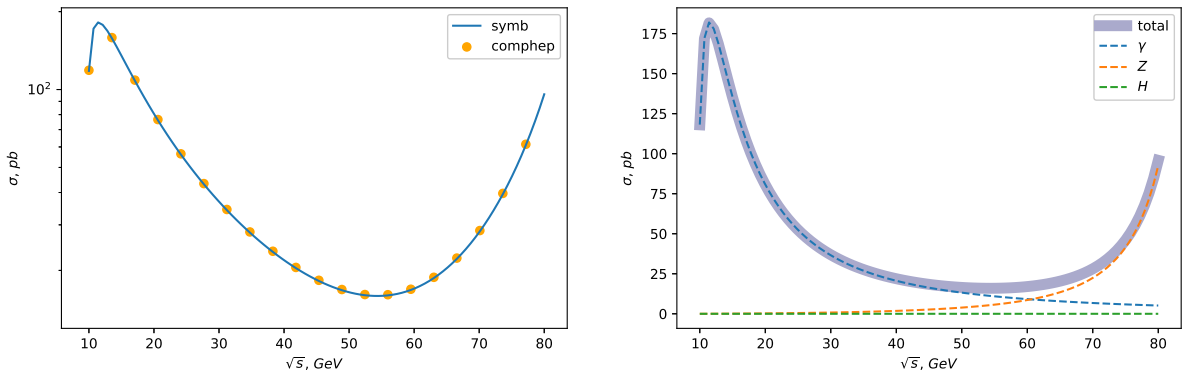

(a) (b)

Figure 3: Total cross section and contributions of various processes at low energies

It can be seen from the low energy plot (see fig. 3) that contribution of the electromagnetic interaction contributes dominantly in the region close to the $b\bar{b}$ threshold, but then decreases quickly. At the same time contribution of Z grows, because at 80 GeV we are getting quite close to the Z's on-shell mass. Also, notice H contribution, it stays comparably suppressed throughout the whole region.

We also want to verify how neglectable are masses of leptons and quarks in this region. For this we plot the total cross section setting $m_\mu = 0$ or $m_b = 0$ explicitly (fig. 4).

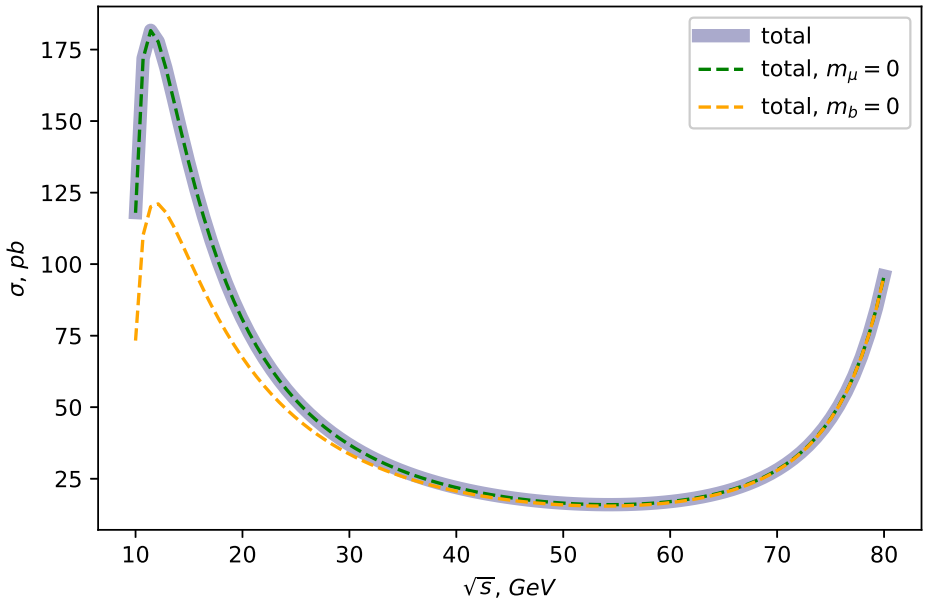

Figure 4: Total cross section with zero mass assumptions at low energeis

Here we discover that we can neglect both mass of muon and b-quark while still catching qualitative behavior of the total cross-section.

After working out some features of low energy behavior, let's investigate the big picture. It is mainly to confirm irrelevance of the Higgs contribution for this process. Peaks are not present on the large scale plot (fig. 5) because the step of the grid is wide and we just jump over the peaks. Since peaks are not the aim of the large scale analysis, we don't try to workaround this issue.

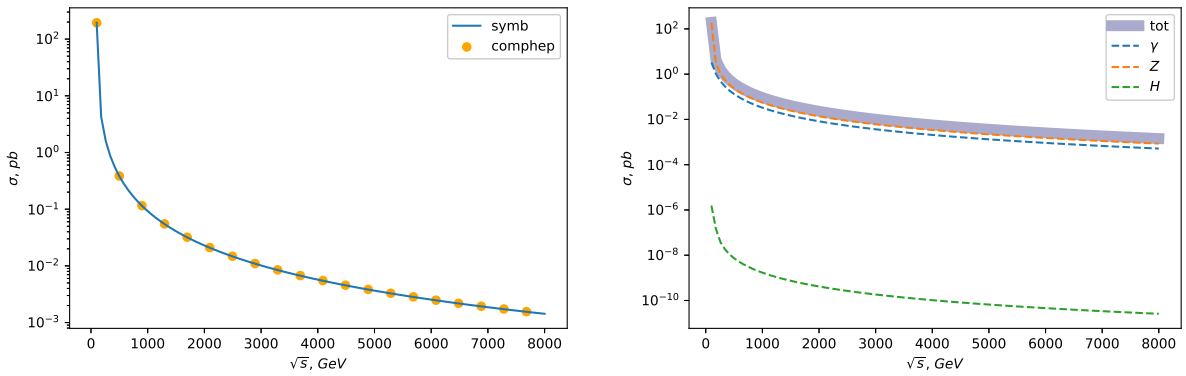

(a) (b)

Figure 5: Total cross section and contributions of various processes at large energies

Now when we've got an idea about the general behavior of different channels contributing to the total cross section, let's focus on the peaks. We plot Z-peak (6) together with the CompHEP prediction, but also we show how essential is decay width of Z around the resonance mass. The total cross section otherwise diverges in this region, so we regularize it by exploiting Breit-Wigner trick.

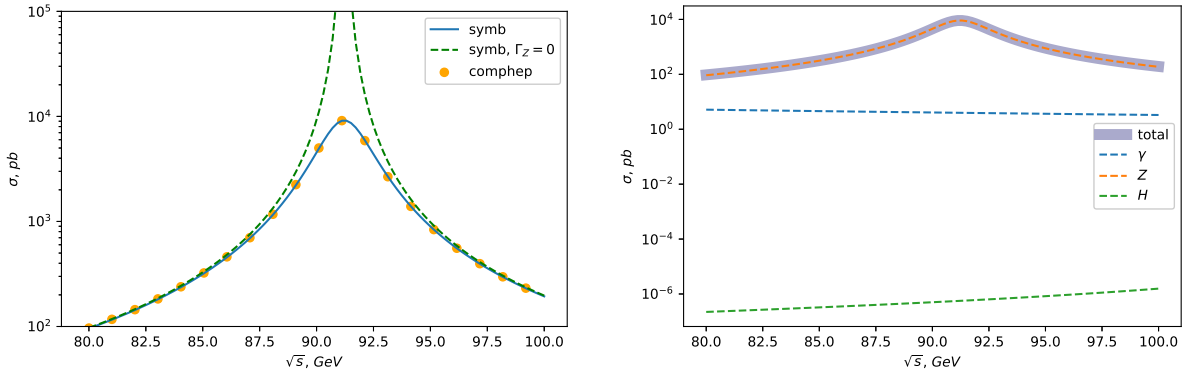

(a) (b)

Figure 6: Total cross section and contributions of various processes around the Z peak

Indeed, around Z peak other contributions look flat and Z-channel contributes dominantly to the shape and the absolute value of the cross section.

Finally, we arrive to Higgs boson peak (fig. 7), and this is the tricky one. It is very narrow, so it is numerically hard to catch it on the grid. We end up with few points appearing on it. Also, notice that Higgs mass we used here is not the well known one, because we tried to fit the CompHEP line, thus we took the CompHEP default mass $m_h = 115\ GeV$. The essential difference between Higgs peak and Z peak is that in case of Z, Z interaction contributes dominantly around the peak, while in the H case Z still provides the baseline while Higgs provides a peak on top.

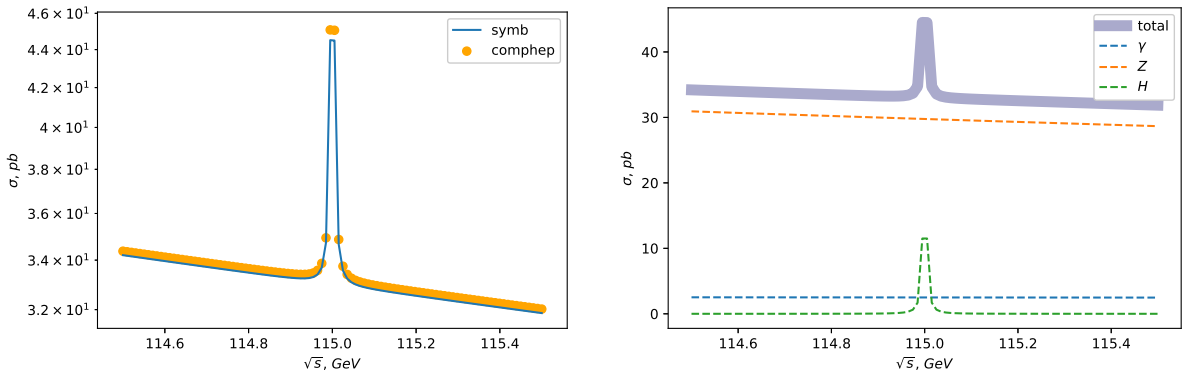

(a) (b)

Figure 7: Total cross section and contributions of various processes around the H peak

Higgs plot closes analysis of the differential cross section.

Forward-backward asymmetry We already discovered some asymmetry between forward and backward direction in the differential cross section plot (fig. 2). The commonly used quantity to describe such an asymmetry looks as follows:

$$A = \frac{\sigma_{\theta>\frac{\pi}{2}} - \sigma_{\theta<\frac{\pi}{2}}}{\sigma_{\theta>\frac{\pi}{2}} + \sigma_{\theta<\frac{\pi}{2}}} \tag{9}$$

We plot this quantity and contributions of different channels to it below. Besides general interest in the character of the asymmetry in this process we also eager to confirm our guess, that the asymmetry being generated by interference terms of Z and γ channels.

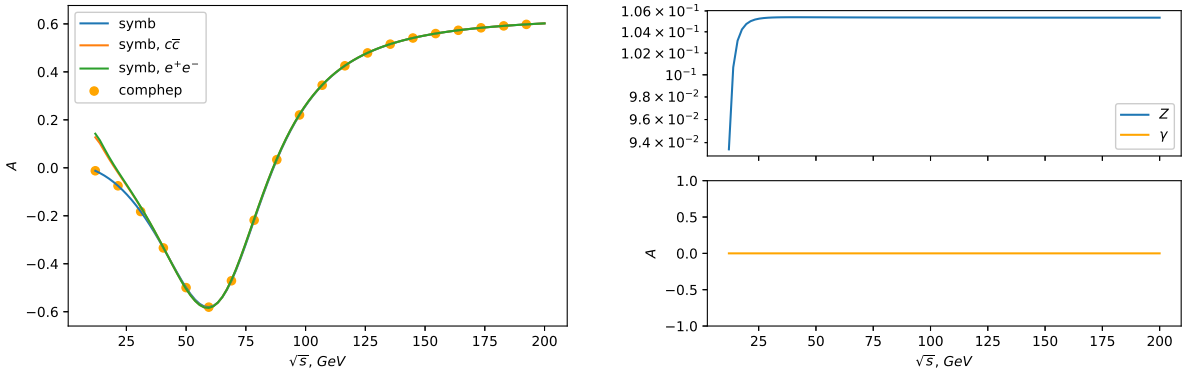

(a) (b)

Figure 8: Forward-backward asymmetry and contributions

Indeed, photon channel doesn't have any asymmetry itself, at the same time at $\sqrt{s} \approx 60\ GeV$ Z has $A \approx 0.1$, but together they generate $A \approx -0.6$ confirming the improtance of the interference term for this quantity.

We also explored asymmetry for alternative final states: e^+e^- and $c\bar{c}$. Both of them are lighter than $b\bar{b}$ and are barely distinguished on the plot, but nonticeably differ from $b\bar{b}$ at the threshold.

New physics. Z' extension For the educational purposes we extend Standard Model with a copy of Z boson, Z', which is completely the same except of the mass. We put mass of Z' to be $m_{Z'} = 300\ GeV$. We then use CompHEP to compare the differential cross section, total cross section and forward-backward asymmetry for two scenarios: with and without Z'.

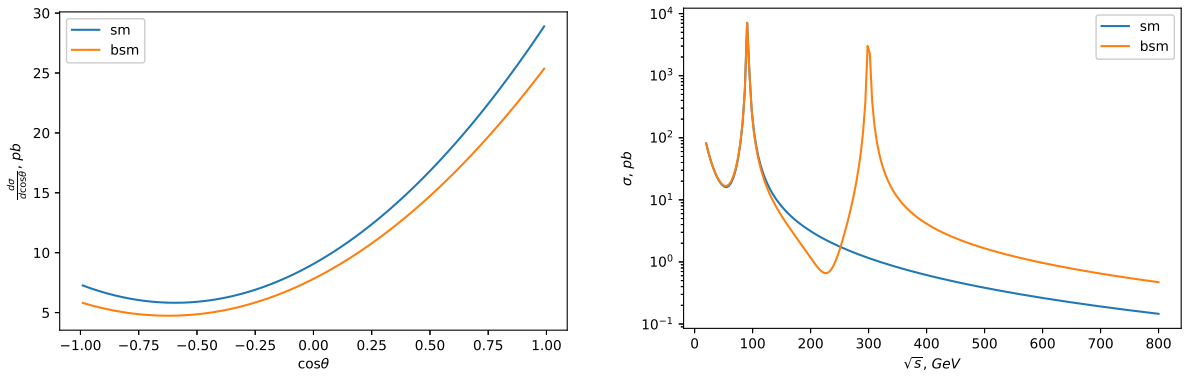

(a) (b)

Figure 9: Comparison of differential and total cross sections for SM and Z' models

Surprising behavior can be observed in the cross-section plots. It turns out that the additional Z' interfers with the SM one destructively giving the smaller cross-section than in the SM case in the region away of Z' mass.

Also we observe an additional dip in the assymetry plot at the resonance mass of Z'. It looks like height of the dip barely depends on the mass of the boson.

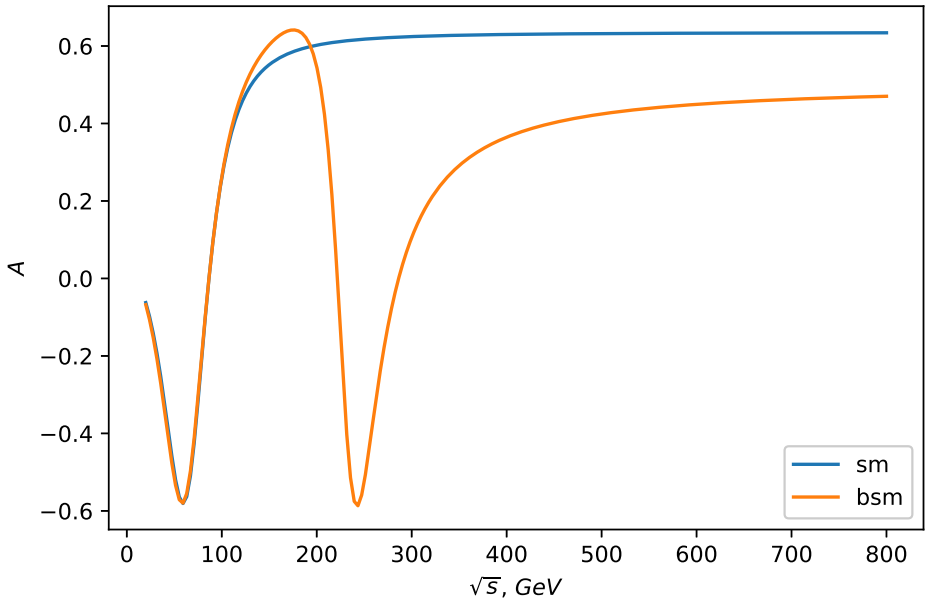

Figure 10: Comparison of the forward-backward asymmetry for SM and Z'

2 ATLAS data analysis

Using ATLAS Open Data [10] we investigated the invariant mass distribution of the $\mu^+\mu^-$ and e^+e^- final states at LHC. Channels contributing to this process were classified into several groups:

- Higgs produced by gluons and vector boson fusion (Higgs)
  - $H \to W^+W^- \to 2l$
  - $H \to ZZ \to 4l$ — although these events suppose to have 4 leptons in the final state, detector might fail and miss few. This contributes to the background then.
- Decays of Z (Zjets)

  - $Z \to \mu^+\mu^-$
  - $Z \to e^+e^-$
  - $Z \to \tau^+\tau^-$
- $t\bar{t} \to W^+W^-b\bar{b} \to 2l$ (ttbar)
- Drell-Yan $q\bar{q} \to Z/\gamma^\star \to 2l$ (DY)
- $WW/ZZ/WZ \to 2l/4l/3l$ (Diboson, Wjets, Zjets)

As a result we've got a stack histogram from the data (based on Even Håland's notebook [13]), showing both MC simulations and data points. There is also a wide peak that can be observed around 90 GeV, it corresponds to Z invariant mass. We won't discover the same peak for W, because two leptons can be produced only by two W bosons:

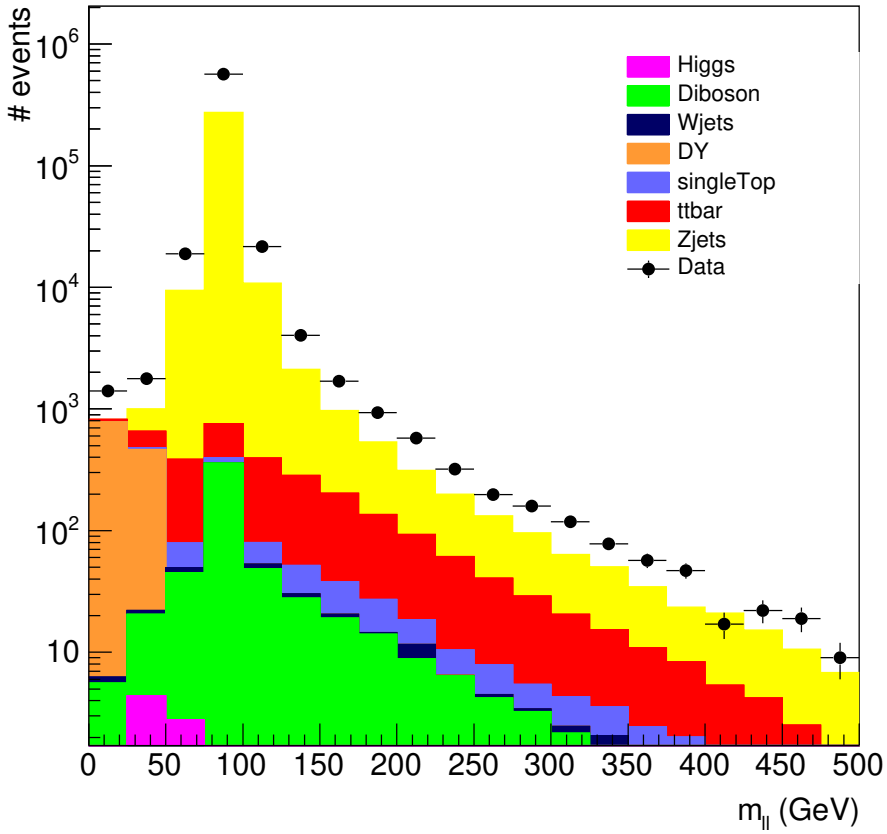

Figure 11: Invariant mass distribution for dilepton final states from CERN Open Data

3 Overview of the publications

There were different kinds of colliders developed throughout the history of particle accelerators. Several of them are relevant to the topic of this project: LEP (Large electron positron collider), Tevatron (Proton-Antiproton collider), LHC (Large Hadron Collider, proton-proton collisions).

Here we provide some relevant publications analysing data from each kind of colliders:

Tevatron ($p\bar{p}$)

- $WH \to l\nu b\bar{b}$ [9]. Here $b\bar{b}$ comes from Higgs decay. It can be relevant to our process as a background generator in the region around Higgs mass.

- $B'\bar{B}' \to b\bar{b} + MET$ [5] A phenomenological research of B' signature at Tevatrona and LHC.
- $b\bar{b} \to 2jets/\mu + jet/\mu\bar{\mu}$ [14]. Another pheno study of $b\bar{b}$ production, also with $\mu\bar{\mu}$ pair signatures.

LEP (e^+e^-)

- $e^+e^- \to b'\bar{b}'$ [4]. Search for the fourth generation of quark with mass $< m_t$. Interesting because of new physics and also involves $ll \to q\bar{q}$ as a main process.
- Extensive conference proceedings on heavy quark physics. Essential part is a talk of P. Dornan (p. 525) on Heavy Quark Physics from LEP. All details of how they have hunted for b quark signatures in e^+e^- collisions. [11]

LHC (pp)

- $H \to ZZ \to llqq$ [2]. Here dilepton final state is being a signature of Higgs decay in proton-proton collisions.
- $ZZ \to ll\nu\nu$ [1]. Quite recent study of ZZ production conducted by ATLAS collaboration. Involves 4 leptons in the final state, but basically it is dilepton $+MET$. For MET analysis knowledge about dilepton behavior is essential.
- $X \to WW \to l\nu l'\nu'$ [3]. Search for BSM heavy particles decaying into WW by analysing dilepton $+MET$ signatures. (ATLAS)

Apparently, dilepton final states are still very important in High Energy Physics analysis. They can play role of gauge boson signatures an constitue background in missing energy studies. While LEP and Tevatron are not active anymore, LHC still operates and delivers results with the help of ATLAS and CMS collaborations.

References

[1] M. Aaboud et al. "Measurement of ZZ production in the final state with the ATLAS detector in pp collisions at $\sqrt{s} = 13$ TeV". In: *Journal of High Energy Physics* 2019.10 (Oct. 2019). ISSN: 1029-8479. DOI: 10.1007/jhep10(2019)127. URL: http://dx.doi.org/10.1007/JHEP10(2019)127.

[2] G. Aad et al. "Search for a heavy Standard Model Higgs boson in the channel $H \to ZZ \to llqq$ using the ATLAS detector". In: *Physics Letters B* 707.1 (Jan. 2012), pp. 27–45. ISSN: 0370-2693. DOI: 10.1016/j.physletb.2011.11.056. URL: http://dx.doi.org/10.1016/j.physletb.2011.11.056.

[3] G. Aad et al. "Search for new phenomena in the $WW \to lnul'nu'$ in pp collisions at sqrt(s) = 7 TeV with the ATLAS detector". In: *Physics Letters B* 718.3 (Jan. 2013), pp. 860–878. ISSN: 0370-2693. DOI: 10.1016/j.physletb.2012.11.040. URL: http://dx.doi.org/10.1016/j.physletb.2012.11.040.

[4] Pankaj Agrawal, Stephen D. Ellis, and Wei-Shu Hou. "Signatures of the $b^{'}$ quark at e^+e^- colliders". In: *Phys. Rev. D* 42 (5 Sept. 1990), pp. 1429–1434. DOI: 10.1103/PhysRevD.42.1429. URL: https://link.aps.org/doi/10.1103/PhysRevD.42.1429.

[5] Johan Alwall et al. "Bs with direct decays: Tevatron and LHC discovery prospects in the bbŕ+ETchannel". In: *Physical Review D* 84.7 (Oct. 2011). ISSN: 1550-2368. DOI: 10.1103/physrevd.84.074010. URL: http://dx.doi.org/10.1103/PhysRevD.84.074010.

[6] Victor Ananyev. *FormSquare applied to muon annihilation process.* URL: https://github.com/vindex10/rbpp-projects/tree/master/project1/scattering/symbolic.

[7] Victor Ananyev. *FormSquare. FORM based routine for computing squared and averaged matrix elements.* URL: https://github.com/vindex10/form-square.

[8] Victor Ananyev. *Visualization for muon annihilation process.* URL: https://github.com/vindex10/rbpp-projects/blob/master/project1/scattering/visualize.ipynb.

[9] Duncan Brown. *Search for $WH \to \ell b\bar{b}$ Final States at the Tevatron.* 2011. arXiv: 1110.2259 [hep-ex]. URL: https://arxiv.org/abs/1110.2259v1.

[10] ATLAS Collaboration. *ATLAS Open Data*. URL: http://opendata.atlas.cern/.

[11] P.J. Dornan. "Heavy quark physics from LEP". In: (Jan. 1997).

[12] E.Boos et al. *CompHEP, a package for evaluation of Feynman diagrams, integration over multi-particle phase space and event generation*. URL: https://theory.sinp.msu.ru/dokuwiki/doku.php/comphep/news.

[13] Even Håland. *Conventional analysis of dilepton final states based on ATLAS Open Data*. URL: https://github.com/Etienne357/FYS5555/tree/master/Conventional_Analysis.

[14] F. Happacher, P. Giromini, and F. Ptohos. "Status of the observed and predictedbb́production at the Fermilab Tevatron". In: *Physical Review D* 73.1 (Jan. 2006). ISSN: 1550-2368. DOI: 10.1103/physrevd.73.014026. URL: http://dx.doi.org/10.1103/PhysRevD.73.014026.

[15] Yorikiyo Nagashima. *Elementary Particle Physics: Foundations of the Standard Model V2*. Wiley-VCH, 2013. ISBN: 3527409661,9783527409662.

[16] Michael E. Peskin and Daniel V. Schroeder. *An introduction to quantum field theory*. Addison-Wesley, 1995. ISBN: 0201503972,9780201503975,0201509342,9780201509342.

[17] M. Tanabashi et al. *Review of Particle Physics*. Vol. D98. 3. 2018, p. 030001. DOI: 10.1103/PhysRevD.98.030001.

[18] Jos Vermaseren. *The FORM project for symbolic manipulation of very big expressions*. URL: https://www.nikhef.nl/~form/.